Cogn Neurodyn (2010) 4:151–163
DOI 10.1007/s11571-010-9103-3

RESEARCH ARTICLE

Synchronized changes to relative neuron populations in postnatal human neocortical development

David L. Cooper · James E. Gentle · Ernest Barreto · James L. Olds

Received: 9 October 2009 / Accepted: 15 January 2010 / Published online: 3 February 2010

Abstract Mammalian prenatal neocortical development is dominated by the synchronized formation of the laminae and migration of neurons. Postnatal development likewise contains "sensitive periods" during which functions such as ocular dominance emerge. Here we introduce a novel neuroinformatics approach to identify and study these periods of active development. Although many aspects of the approach can be used in other studies, some specific techniques were chosen because of a legacy dataset of human histological data (Conel in The postnatal development of the human cerebral cortex, vol 1–8. Harvard University Press, Cambridge, 1939–1967). Our method calculates normalized change vectors from the raw histological data, and then employs *k*-means cluster analysis of the change vectors to explore the population dynamics of neurons from 37 neocortical areas across eight postnatal developmental stages from birth to 72 months in 54 subjects. We show that the cortical "address" (Brodmann area/sub-area and layer) provides the necessary resolution to segregate neuron population changes into seven correlated "*k*-clusters" in *k*-means cluster analysis. The members in each *k*-cluster share a single change interval where the relative share of the cortex by the members undergoes its maximum change. The maximum change occurs in a different change interval for each *k*-cluster. Each *k*-cluster has at least one totally connected maximal "clique" which appears to correspond to cortical function.

Keywords Sensorimotor · Network clique · Broca's area · Primary visual cortex · Retrosplenial cortex

Electronic supplementary material The online version of this article (doi:10.1007/s11571-010-9103-3) contains supplementary material, which is available to authorized users.

D. L. Cooper
Doctoral Program in Neuroscience, George Mason University, Fairfax, VA 22030, USA

J. E. Gentle
Department of Computational and Data Sciences, George Mason University, Fairfax, VA 22030, USA

E. Barreto
Department of Physics & Astronomy, the Krasnow Institute for Advanced Study, George Mason University, Fairfax, VA 22030, USA

J. L. Olds (✉)
Department of Molecular Neuroscience, Krasnow Institute for Advanced Study, George Mason University, 4400 University Dr., Fairfax, VA 22030, USA
e-mail: jolds@gmu.edu

Introduction

The role of Layer I and *reelin* in the prenatal formation of mammalian neocortical laminae (Bar and Goffinet 2000) is well known, as is the pattern of lateral migration of interneurons targeted to specific neocortical areas (Letinic et al. 2002). These and other control factors, such as *bmp*, *shh*, and the homeobox genes appear to follow a basic developmental template shared by vertebrates to which the mammalian modifications have been added (Gallego-Diaz et al. 2002; Kolpak et al. 2005; Holland and Takahashi 2005). Furthermore, the consensus is that the template employs highly conserved genetic and epigenetic factors to provide the necessary coordination of neurodevelopment (Noden 1991). Human neocortical development is consistent with this pattern to the extent that neuron versus non-neuron cell counts in human brains have the same relationship to body weight as for primates in general,

whereas the great apes such as gorillas apparently have over-sized bodies (Azevedo et al. 2009).

Developmental studies in animals with high temporal resolution reveal that a neuron's birth cohort is the best predictor of cell-fate during prenatal development (Takahashi et al. 1999). During postnatal development, neuron death (pruning) putatively replaces neurogenesis as the major factor defining the structure of cortical neuronal populations (Stiles 2008). Postnatal histogenic cell death does not recapitulate the prenatal sequence of laminar development (Verney et al. 2000), but rather seems to be a neurotrophin- and activity-dependent process in which neuron survival hinges on successful synapse formation with target cells (Huang and Reichardt 2001). This pruning, in conjunction with synapse elimination, might be an efficient developmental process that matches projection cells to target cell populations, but cell death may also serve other functions, such as the elimination of transient structures or error elimination (Stiles 2008).

Studies of animal postnatal development provide examples of so-called "sensitive periods" when functions such as ocular dominance must be established (DiCristo et al. 2007). Sensitive periods for complex cognitive functions such as human language are also well-reported (Ross and Bever 2004; Marcotte and Morere 1990). In these examples, the animal or human subject interacts with external stimuli as cognitive resources (neurons) become committed to a particular function. Insufficient stimulation can result in the diversion of cognitive resources to alternative functions (Michel and Tyler 2005).

The present neuroinformatics analysis supports the notion that functional, activity-based postnatal alignment of cortical areas occurs at the level of synchronized changes at specific *addresses*. By address, we mean a specific layer within a particular Brodmann area, e.g., BA 44 LV. We suggest that both the area and layer component of the address are important. Given the clear relationship between function and Brodmann area (Rakic 1988, 2001), one would hypothesize that a Brodmann area would be predictive of neuron population dynamics during postnatal cortical development. At the same time, Nomura et al. (2008), showed in a comparative study of the mammalian and avian pallium that most control mechanisms are highly conserved in evolution, including *reelin*-dependent neuronal migration in mammalian corticogenesis. Thus, if the conserved neurogenetic and neuromigration factors that lead to laminar fate (Takahashi et al. 1999) as well as to corollary cell death mechanisms (Gohlke et al. (2007) continue to operate after birth, one would also hypothesize that the neocortical laminar identity would be a predictor of the course of postnatal neocortical neurodevelopment as well.

For human subjects, histological evidence from children to examine these hypotheses is scarce. However, Conel's study (1939–1967) of the development of the human cortex provides a uniquely comprehensive dataset of neuron populations using a common framework and methodology for 54 human subjects whose deaths were distributed across eight neurodevelopmental observation ages ranging from birth to 72 months ($5 \leq N \leq 9$ for each observation age). Conel's data permit a comparison of 37 neocortical areas in the left hemisphere across all of these neurodevelopmental stages.

Here, we show evidence that synchronized neurodevelopmental changes occur at the address level in cortical neuron populations. These results support the hypothesis that for human subjects postnatal activity-dependent mechanisms (laminar-neocortical area interactions) are superimposed on a combination of the previously established animal model pre-natal control mechanisms (such as laminar development) to coordinate neocortical neuronal populations over the studied neurodevelopmental time course. Moreover, the emergence of functionally related neuron changes prior to much of the overt cognitive activity related to those functions implies that these synchronized changes have both an internal, clock-like, basis as well as an activity basis.

Materials and methods

(a) Conel's data

The current neuroinformatics analysis depends on the massive dataset of post mortem histological observations collected by Conel (1939–1967). Conel remains one of the few sources for histological data on a systematic, structural basis (Azevedo et al. 2009). However, his data is massive only in the sense of detail at each observation age, not in the sense of large numbers of subjects at each age (see "A Cautionary Tale" in the "Supplement data").

Notwithstanding his reputation as an accomplished clinical neuroanatomist, for his study of human neocortical development, Conel did not report the precise cause of death for any of the 54 subjects. However, he did explicitly state that the cause of each subject's death was *unrelated* to neurodevelopment. While the field of human clinical neuroanatomy has changed since Conel collected his data, for the purposes of this neuroinformatics study we assume Conel's assertion to be valid.

Using classic histological techniques, Conel recorded a *mean* neuronal density value based on 30 separate cresyl violet-stained tissue samples from each subject within specific area-layer combinations (we term these combinations *addresses*). In addition, he recorded the corresponding mean

across individuals at each observation age ($5 \leq N \leq 9$; total $N = 54$), for 37 neocortical areas in the left cerebral hemisphere. Conel's procedure avoids possible stereological error from a single soma contributing to adjacent slices (Abercrombie 1946). As has been reported, the number of cresyl violet-stained somata provides an accurate marker for the neuron population (Pilati et al. 2008). Azevedo et al. (2009) uses cresyl violet to calibrate an automated method for counting neurons using fluorescent DNA-tagged brain tissue. Our overall strategy in the present work was to use the Conel cresyl violet-stained human neocortical tissue to reveal information about neuron densities during the neurodevelopmental series of observations from birth to 72 months.

(b) Analysis of Conel's data

Neuroinformatics analysis of this data was conducted in three phases. First, we calculated neuron population from Conel's neuron density and layer thickness measurements. Second, using the normalization steps described in Eqs. 1–3 below, population *change vectors* were defined by Eq. 8. These change vectors defined developmental trajectories. Third, *k*-means cluster analysis of the developmental trajectories of all 222 addresses from birth to 72 months was performed. These are described in detail below.

Phase 1: neuron population

In our method, the neuron population $v(l, b, t)$, for neocortical layer l, Brodmann area b and observation age index t, is Conel's reported mean density for that address multiplied by the layer depth (in 0.1 mm increments). v represents the number of neurons in a "sample count" with base 100 μm^2 that spans the neocortical layer reported in that measurement. These calculations are summarized in Fig. 1 in "Results". The six sample counts for the addresses in each Brodmann area, when summed, constitute a *sample column*. For each fixed t, Conel's data include observations on each of several individuals for various values of l and b. The data at the different values of t, however, were from different subjects.

Input values for $v(l, b, t)$ were carefully cross-checked for accuracy with the raw tabular values for neuron density and layer depth in the CYBERCHILD data base (Shankle et al. 2000). CYBERCHILD represents an important neuroinformatics resource, as it provides computerized database access to the entire Conel corpus. Our input population values differ from CYBERCHILD for 72 months values, as CYBERCHLD lists an average of left and right hemisphere values for each address, whereas we have used left hemisphere data exclusively since Conel did not make observations on

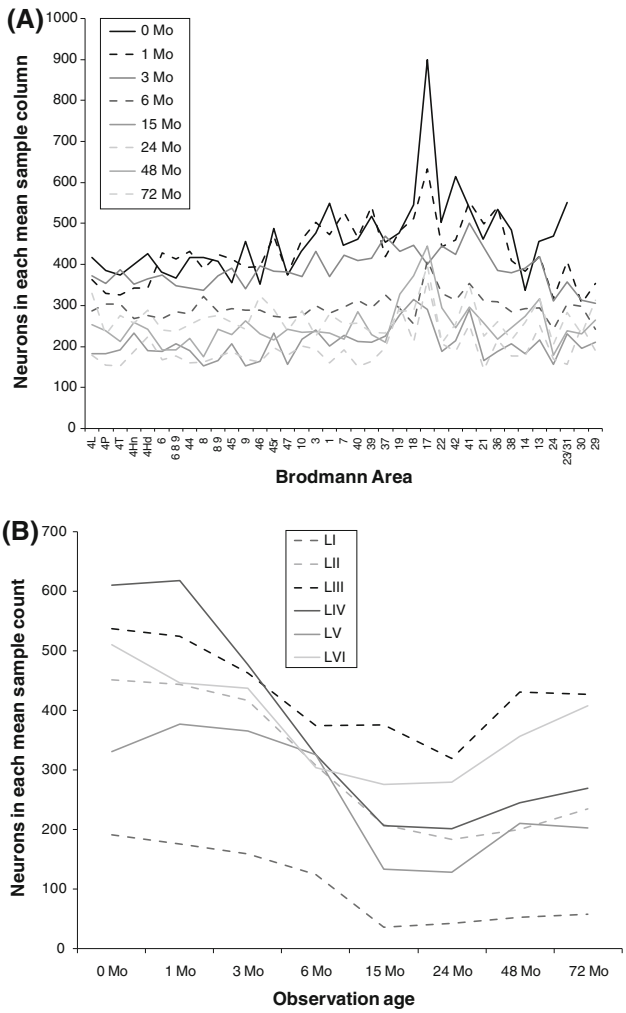

Fig. 1 Mean raw neuron population by area, layer and age in Conel. Raw population values have not been adjusted for shrinkage in either panel. **a** Mean sample column neuron population by Brodmann area by observation age, with the mean taken over the six layer samples in the respective Brodmann area. The curve for 0 months reflects missing data, since Conel did not report values for BA 29 and 30 at that age. The raw mean neuron population over all sample columns declines from 463.5 at birth to 249.5 at 48 months. At 72 months it is 266.3. The greatest absolute decline in mean neuron population, 95.9 per sample column, takes place between 3 and 6 months. The greatest relative decline in mean neuron population (24.55%) takes place between 6 and 15 months. **b** Mean raw sample counts averaged over each neocortical layer by observation age, with the mean taken over the samples of all Brodmann areas within a given layer. The mean declines from 438.4 at birth to 192.3 at 48 months. At 72 months it is 266.5. The greatest absolute decline in mean neuron sample count, 92.9 per layer, takes place between 3 and 6 months. The greatest relative decline in mean neuron sample count (29.91%) takes place between 6 and 15 months

neuron density in the right hemisphere except at the 72 months time point in neurodevelopment. Our calculated populations also differ from CYBERCHILD for Layer V; this is because our method for calculating mean neuron density over Conel's reported sublayers for Layer V differs from that of Shankle et al. (see "Supplement data").

Phase 2: population change vectors

For our analysis of relative population changes at each neocortical *address* from birth to 72 months, we first normalized neuron populations at each observation age index $t = 1, \ldots, 8$, corresponding to observation ages 0, 1, 3, 6, 15, 24, 48 and 72 months, respectively.

$$\begin{aligned} R(l,b,t) &\equiv \frac{1}{37}\sum_{i=1}^{37}\log\left(\frac{v(l,b,t)}{v(l,i,t)}\right) \\ &= \log v(l,b,t) - \frac{1}{37}\sum_{i=1}^{37}\log(l,i,t) \\ &= \log v(l,b,t) - \langle \log v(l,i,t)\rangle_i \end{aligned} \tag{1}$$

This procedure normalizes the raw population calculation $v(l, b, t)$ as a relative count over all Brodmann areas for each layer. Thus, the values of $R(l, b, t)$ from Eq. 1 reflect the average log ratio of the number of neurons in a sample count relative to the number of neurons in all other sample counts within a given layer averaged across all subjects at a particular observation age. This relative measure within layer b at age index t solves an important problem. Conel followed von Economo's counting method, which is subject to a systematic proportional overcount (Conel 1939; von Economo and Koskinas 1925). Such a systematic proportional overcount does not affect the calculated normalized ratios described above.

Subsequently, changes in $R(l, b, t)$ were normalized between observation ages. Calculating this second normalization function requires defining the sample variance of $v(l, b, t)$ for the pooled Brodmann areas in each layer at each observation age. The sample variance is given by

$$s^2(l,t) = \frac{1}{37}\sum_{i=1}^{37}\left[\log v(l,i,t) - \langle \log v(l,b,t)\rangle_b\right]^2 \tag{2}$$

In Eq. 3, we define the change $C(l, b, t)$ at each address (l, b) as the squared difference between $R(l, b, t)$ and $R(l, b, t + 1)$ divided by the pooled sample variance for each layer l at t and $t + 1$. The interval between t and $t + 1$ is called a "change interval," where the data at t and $t + 1$ were from different subjects.

$$C(l,b,t) = \frac{[R(l,b,t) - R(l,b,t+1)]^2}{s^2(l,t) + s^2(l,t+1)} \tag{3}$$

$C(l, b, t)$ is defined over seven change intervals for Conel's data, beginning with the first interval between newborn to 1 month. With 222 addresses and seven change intervals, there are a total of 1,554 values for $C(l, b, t)$ described in the histogram in Fig. 2 and Table 3 in "Results". If we assume that $R(l, b, t)$ is normally distributed for each t, because the data are from different individuals (and hence, independent), then $C(l, b, t)$ in Eq. 3

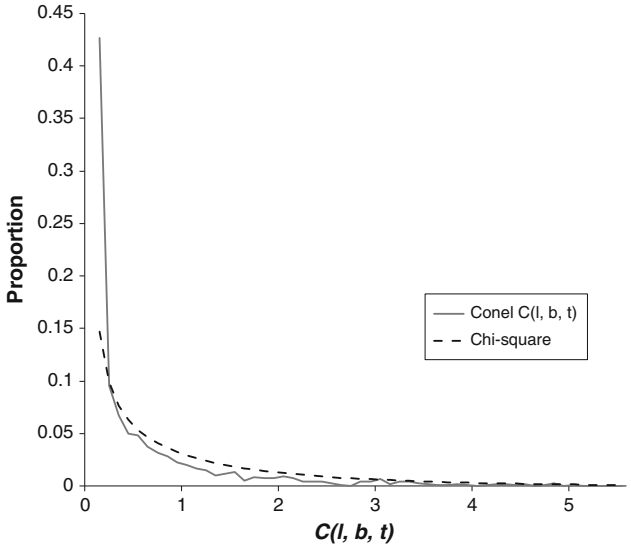

Fig. 2 Distribution of normalized change interval magnitudes. Distribution of $C(l, b, t)$ values for all seven change intervals. $N = 1{,}554$ overall, $N = 9$ for $C(l, b, t) > 5.5$ (not shown). Histogram bins are in increments of 0.1 units. Rather than the predicted Chi-square distribution with one degree of freedom (also shown), the histogram in this figure is well-described by a gamma distribution ($P = 0.99997$, Kolmogorov–Smirnov test; parameters $\alpha = 0.3638$, $\beta = 1.6570$ and mean $= 0.6028$)

would be a Chi-square random variable with one degree of freedom. More precisely, begin with the null hypothesis that $R(l, b, t) = R(l, b, t - 1)$, abbreviated as R and R_0, respectively. That is, according to the null hypothesis the relative share of cortical neurons at address (l, b) for the subject population at time t is the same share as for the different subject population but same address at the previous time $t - 1$. Define the likelihood ratio λ

$$\lambda = \frac{L_{\max}(\omega)}{L_{\max}(\Omega)} \tag{4}$$

where $L_{\max}(\omega)$ is the maximum likelihood for the null hypothesis, and where $L_{\max}(\Omega)$ is the maximum likelihood of $R(l, b, t)$ in general. This is a case of a nested hypothesis as required by Wilks (1962: 419–421). Then,

$$-2\log\lambda \approx -(R - R_0)^2\frac{\mathrm{d}^2}{\mathrm{d}R^2}\log L \tag{5}$$

where L is the likelihood of $R(l, b, t)$. Using the Cramér-Rao bound

$$\mathrm{Var}(R) \sim \frac{-1}{E\left(\frac{\mathrm{d}^2}{\mathrm{d}R^2}\log L\right)} \tag{6}$$

Equation 5 simplifies to

$$-2\log\lambda \approx \frac{(R - R_0)^2}{\mathrm{Var}(R)} \tag{7}$$

This is asymptotically Chi-square with one degree of freedom with increasing n, where $n = 222$ for Conel for each change step and $n = 1{,}554$ for the entire Conel data set (for a general discussion of the $-2 \log \lambda$ statistic see Ewens and Grant 2001: Sect. 8.4.2). Using the pooled variance for each change step as defined in Eq. 2, the $-2 \log \lambda$ statistic becomes $C(l, b, t)$, which is thus also approximately Chi-square with one degree of freedom.

The null hypothesis predicts that $C(l, b, t)$ derived from Conel's data is Chi-square with one degree of freedom. If it is not, there is evidence to reject the null hypothesis. We use the Kolmogorov–Smirnov (KS) goodness-of-fit test for this step. For statistical tests related to individual magnitudes of $C(l, b, t)$, we can also test against a Chi-square distribution with one degree of freedom, in this case using the cumulative probability distribution. Since values of $C(l, b, t) > 3.9$ have $P < 0.05$ using this one-tailed test, they are statistically significant regardless of the precise distribution of the actual raw Conel data.

Equation 8 then defines a normalized seven-dimensional population "change vector" $\vec{P}$ for the entire developmental trajectory (newborn to 72 months) for each address (l, b). The "change indices" from 1 to 7 define the successive change intervals between age indices t, where 1 is the change interval between birth and 1 month and 7 is the change interval between 48 and 72 months. For convenience in calculations for the k-means cluster analysis below, $\vec{P}$ is defined as a row vector. Each element in $\vec{P}$ represents measurements on a different sample of subjects.

$$\vec{P}(l, b) = [C(l, b, 1)C(l, b, 2) \cdots C(l, b, 7)] \tag{8}$$

To assess and visualize area, layer and change interval interactions from birth to 72 months, we then employed k-means cluster analysis of the *change vector* data, using the 222 row vectors resulting from the six neocortical layers and 37 Brodmann areas. Each change vector $\vec{P}$ (l, b) has seven normalized components $C(l, b, t)$ for each observation change interval t. In "Results" or "Discussion", if the change interval is not completely specified (e.g., "from 3 to 6 months"), the change interval will be labeled with the final observation age for that change interval (e.g., "6 months"). The normalization steps in Eqs. 1–3 transform raw sample count changes into changes in relative population share across the cortex. This enabled us to identify synchronized changes to neuron populations by using k-means cluster analysis.

Phase 3: K-means cluster analysis of population change vectors

The purpose of k-means cluster analysis is to separate a group of data points into k clusters, where the value of k is optimized given the definition of an appropriate separation distance. We will refer to these as k-clusters. We first assessed the appropriate value for k with the mean cluster separation values summarized in Table 2 in "Results", using 1,000 replications for each value of k ranging from 2 to 12 to eliminate local minima. The value of k is optimal when the mean k-cluster separation is maximal. To associate correlated developmental trajectories in the clusters, the separation distance was calculated using the correlation distance between the $\vec{P}$ vectors defined by Eq. 8. For $\vec{P}_x(l_x, b_x)$ and $\vec{P}_y(l_y, b_y)$, the correlation distance between $\vec{P}_x$ and $\vec{P}_y$ is defined as 1 minus the sample correlation, r, between the points treated as sequences of values and is made explicit below in Eq. 9. By definition, when $\vec{P}_x$ and $\vec{P}_y$ are completely uncorrelated, $r = 0$ and $D(\vec{P}_x, \vec{P}_y) = 1$, abbreviated as $D = 1$. When $r = 1$, $D = 0$. When $r = -1$, $D = 2$.

$$D(\vec{P}_x, \vec{P}_y) = 1 - \frac{7\sum_{i=1}^{7} C_x(l_x, b_x, i)C_y(l_y, b_y, i) - \sum_{i=1}^{7} C_x(l_x, b_x, i)\sum_{i=1}^{7} C_y(l_y, b_y, i)}{\sqrt{7\sum_{i=1}^{7} C_x(l_x, b_x, i)^2 - \left(\sum_{i=1}^{7} C_x(l_x, b_x, i)\right)^2}\sqrt{7\sum_{i=1}^{7} C_y(l_y, b_y, i)^2 - \left(\sum_{i=1}^{7} C_y(l_y, b_y, i)\right)^2}} \tag{9}$$

The set of k-clusters accounts for all developmental trajectories for the 222 addresses in Conel's data. To analyze each k-cluster for potential biological function, we then examined the relational networks defined for $D < 0.1$ (or $r > 0.9$ within each cluster) in terms of the $C(l, b, t)$ components of their respective change vectors. Within these highly correlated relational networks, we further isolated the maximal "cliques," or totally connected networks that are subsets of the undirected network graph for $D < 0.1$ (Godsil and Royle 2004). Several k-clusters had more than one clique of maximal size. In "Results" and "Discussion", we refer to the addresses in the one or more maximal cliques as the "core" for each respective k-cluster.

To test whether the single spike per k-cluster pattern in the radar plot in Fig. 4 was an artifact of the k-means

method applied to seven change intervals, we constructed an empirical cumulative distribution function (cdf) characterizing k-cluster graphs randomly generated by a Monte Carlo process. For this type of Monte Carlo test, 1,000 iterations are more than sufficient (Gentle 2002). Each iteration began with a 222 × 8 table of random numbers drawn from the unit interval, corresponding to a null hypothesis that neuron populations are equiprobable. Equations 1–3 were then applied to the table and the resulting change vectors were clustered using the k-means algorithm with $k = 7$ using Eq. 9 to define the distance metric. Let $m(k, t) = \text{mean}[C(l, b, t)]$ for each of the k-clusters in a given change interval resulting from these calculations. After sorting, we then used the statistic $s(t) = \max[m(k, t)]/\text{mean}[m(k, t)]$ to characterize each change interval in the graph, and mean(s) to characterize the graph across all change intervals. Using the results from 1,000 iterations, the surrogate cdf then allowed us to estimate a P value for the actual Conel data. MATLAB code for Eqs. 1 and 3, as well as this Monte Carlo characterization of random graphs is included in the "Supplement data".

Results

Figure 1a shows the mean sample count, or mean neuron population by layer and observation age in Conel, uncorrected for shrinkage. Figure 1b shows the corresponding mean neuron population for each layer as calculated from values for each of the 37 Brodmann areas in the dataset. A sample count is calculated for a volume with a base of 100 μm^2 that spans the respective cortical layer (see "Methods").

Table 1 shows the optimal value for k in the k-means cluster analysis by maximizing the mean cluster separation distance using the correlation distance defined by Eq. 9 in "Methods". The optimal separation distance occurs when $k = 7$, corresponding to seven" k-clusters." As noted in "Methods", $D = 1$ corresponds to no correlation ($r = 0$).

Figure 2 shows the distribution resulting from the normalization steps in Eqs. 1–3 in "Methods". It depicts the distribution of all $C(l, b, t)$ values except nine values >5.5 that are included in Table 2, which lists all 24 statistically significant addresses with $C(l, b, t) > 3.9$. The distribution of $C(l, b, t)$ in Fig. 2 is not the expected Chi-square distribution with one degree of freedom ($P = 0.0112$, KS test). As noted in "Methods", this supports the alternative hypothesis that $C(l, b, t + 1)$ is different from $C(l, b, t)$ for some addresses (l, b) for at least one change interval.

Figure 3 shows the distribution of all 222 addresses into k-clusters. The k-clusters are groups of addresses whose change vectors are most closely aligned using the correlation distance in Eq. 9 in "Methods" as the metric. The number of each cluster is arbitrary, as assigned by the k-means algorithm during 1,000 replications (see "Methods").

Table 1 Mean cluster separation distance for different numbers of clusters

Number of clusters	Mean cluster separation
2	0.2769
3	0.3386
4	0.3778
5	0.4121
6	0.4439
7	0.4767
8	0.4514
9	0.4501
10	0.4271
11	0.4236
12	0.415

Distance metric is the correlation distance (Eq. 9 in "Methods")

A maximal clique in a k-cluster is the largest set of totally connected addresses in the cluster. Defining a connection as a relationship between addresses x and y, where $D(\vec{P}_x, \vec{P}_y) < 0.1$ in Eq. 9 in "Methods" (or correlation $r_{xy} > 0.9$), 11 of the 24 outliers in Table 2 belong to the maximal clique in their respective k-cluster, indicated by an asterisk (sample correlation $r = 0.8192$, $P = 0.0242$, two-tailed t-test against the null hypothesis that the distribution by change interval of the 11 maximal clique members and the 24 significant $C(l, b, t)$ values are from different distributions).

Figure 4 shows the mean value of $C(l, b, t)$ for each of the seven k-clusters as a radar plot graph. There is a one-to-one correspondence between a maximum change vector component in a k-cluster and each of the seven change intervals.

Figure 5 shows the relational network for the first k-cluster (K-1), where $D < 0.1$. The figure depicts all members of K-1. There is only one totally connected maximal clique (with nomenclature from Conel): BA 6 LVI (posterior supplemental motor area of the gyrus frontalis superior), BA 45 LIV (inferior gyrus frontalis medialis/pars triangularis), BA 22 LI (area temporalis superior), and BA 24 LIII (area limbica anterior agranularis of the gyrus cinguli).

We define the "core" of a k-cluster to be the set of addresses contained in its maximal cliques. In the case of K-1, the core consists of a single maximal clique of size four. Figure 6 reveals the $C(l, b, t)$ values for the core, as well as the mean core values compared to the entire cluster.

Table 2 Statistically significant values of $C(l, b, t)$

1 Mo	29 LI	29 LIV						
	4.4938	4.1803						
3 Mo	17 LIII	17 LV	**38 LI***	4T LV				
	10.8246	7.0145	4.9739	4.239				
6 Mo	**29 LVI***	17 LIII	**17 LI***					
	16.6004	6.4275	6.254					
15 Mo	**4P LVI***	**29 LV***	**18 LII***	41 LI	**8 LIII***	**4Hd LVI***	10 LI	**21 LII***
	7.1081	6.6642	6.5119	4.8475	4.8088	4.7902	4.4962	4.3299
24 Mo	**14 LI***	**42 LVI***						
	5.7625	4.442						
48 Mo	45r LI							
	4.7949							
72 Mo	45r LI	10 LI	22 LVI	23/31 LIII				
	4.7137	4.4902	4.267	4.0839				

Change interval, address (Brodmann area and layer) and $C(l, b, t)$ value are indicated. Asterisks and bolding denote the addresses that belong to a maximal clique in a k-cluster. Nine addresses with $C(l, b, t) > 5.5$ were not included in Fig. 2. Altogether, 24 values of $C(l, b, t)$ were statistically significant ($P < 0.05$, one-tailed test against Chi-square cdf, one degree of freedom)

T trunk, *P* paracentral lobule, *Hd* head, *r* rostral

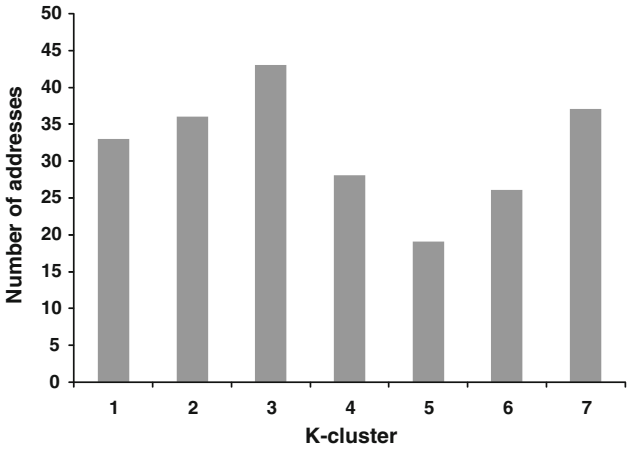

Fig. 3 Distribution of neocortical addresses into seven k-clusters ($N = 222$). Table 1 showed that the optimal number of clusters for the k-means algorithm was 7. The distribution of the 222 change vectors in Conel's data from Eq. 8 was then sorted into seven k-clusters by the algorithm using Eq. 9 as the distance metric for cluster membership and separation of the clusters. Addresses with the most highly correlated changes in their respective values for $C(l, b, t)$ were assigned to the same k-cluster. Cluster number was assigned arbitrarily by the k-means algorithm

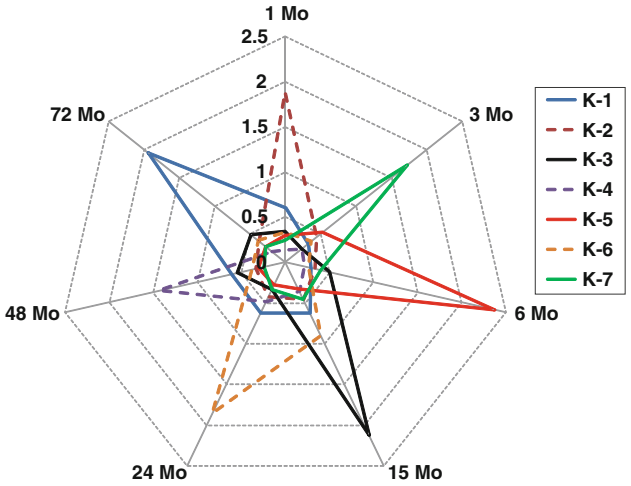

Fig. 4 Correspondence of k-cluster to change interval. *Radar plot axes* indicate mean $C(l, b, t)$ values for the respective k-clusters. Radial axes are the seven change intervals. Each of the k-clusters has a maximum on a unique change interval axis. Using a Monte Carlo process to construct an empirical cumulative probability distribution function (cdf) for randomly generated graphs of seven k-clusters using a "mean max-over-mean" statistic for each graph (see "Methods"), the relative size of the maxima and their one-to-one distribution across the change intervals in this figure is statistically significant ($P \approx 0.001$ from the empirical cdf; the sample mean Monte Carlo graph statistic was 2.845 ± 0.104 (sample standard deviation for $N = 1{,}000$). The same statistic for the Conel data was 3.180)

The mean cluster $C(l, b, t)$ values are the same as those as in Fig. 4.

The largest k-cluster in the Conel data is K-3. It also has the largest core, with two maximal cliques of size nine. Eight of the addresses in these maximal cliques overlap, as shown in Fig. 7. Thus, the core contains ten addresses. The "unique" nodes on this graph are BA 29 LV (area retrosplenialis granulosa) and BA 8 LIII (medial gyrus frontalis superior in von Economo's area frontalis intermedia). They are "unique" in the sense of being totally connected to eight other addresses, but not to each other.

Figure 8 shows the core $C(l, b, t)$ and mean $C(l, b, t)$ values for K-3. The two maximum values in Fig. 8a, BA 4P LVI (the paracentral lobule portion of BA 4) and BA 29 LV are both outliers in Table 2. However, the correlated

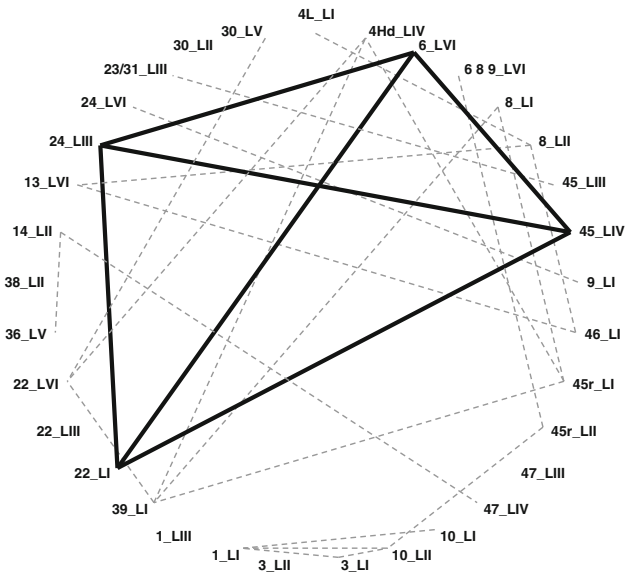

Fig. 5 Relational graph and maximal clique of the first *k*-cluster (K-1) for $D < 0.1$. The 33 addresses in K-1 are listed in clockwise order from BA 4L Layer I at the top to BA 30 Layer V. The order is the one used by Conel, generally proceeding from frontal lobe to the parietal, occipital, temporal lobes, and then medial cortical areas. *Dashed lines* show all instances where $D < 0.1$. The *solid bold lines* show the maximal clique for the cluster, which has size four. Only K-1 and K-4 have single maximal cliques of size 4. K-5 and K-6 have more maximal cliques of size 4. K-2 and K-7 have two overlapping maximal cliques of size 6, and K-3 has two overlapping maximal cliques of size 9. Abbreviations: L = leg; Hd = head; r = rostral

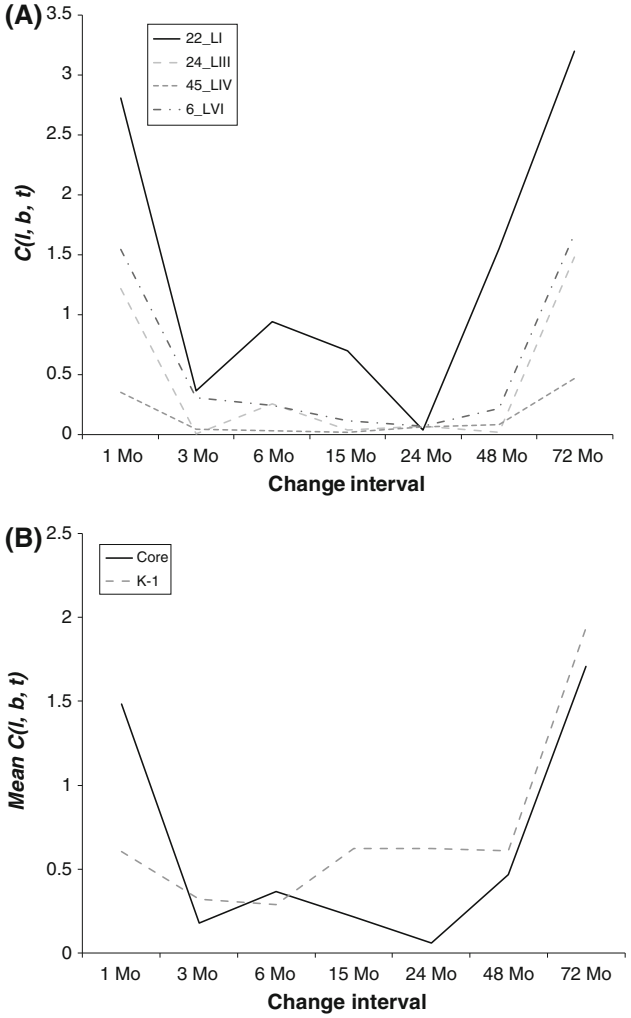

Fig. 6 $C(l, b, t)$ values for K-1 and the K-1 core. **a** $C(l, b, t)$ for the four members of the single maximal clique. This is a graph of the entire trajectory for each of the four addresses in the K-1 core, by $C(l, b, t)$ and change interval. The secondary peak $C(l, b, t)$ values for 1 month provide a relatively complex overall trajectory for this group of addresses. **b** Mean $C(l, b, t)$ for the core compared to mean $C(l, b, t)$ for the entire cluster. The mean trajectory for the entire *k*-cluster has a much lower value for 1 month compared to the mean for the core addresses, making the core addresses a relatively distinct sub-set of a *k*-cluster with correlated maximal $C(l, b, t)$ values at 72 months

trajectories in the K-3 core also include BA 19 LIV (area peristriata) which also has a maximum of 0.7003 at 15 months. The remaining core areas have $C(l, b, t)$ maxima at 15 months between 0.7003 and 7.1076, reflecting correlations on multiple change scales. The comparison of mean $C(l, b, t)$ values for the core and the *k*-cluster as a whole in Fig. 8b reflects greater homogeneity among the change vector trajectories than in K-1.

Corresponding figures for the remaining *k*-clusters are included as a supplement. Maximal clique sizes and descriptions for all clusters are summarized in Table 3. There are seven maximal cliques of size four distributed among four of the *k*-clusters. There are four maximal cliques of size six, two in K-2 and two in K-7. There are two maximal cliques of size nine in K-3. Thus, there are 47 addresses in the seven *k*-cluster cores. They belong to 27 Brodmann areas. BA 6 has four addresses in different cores. No other Brodmann area has more than two addresses in any core.

Discussion

The principal result of this paper is the one-to-one correlation between large change steps in successive neuron populations and observation age in human neocortical development to age six. Change steps are normalized measures of relative neuron population shares at individual area/layer addresses. The pattern of synchronized change in Fig. 4 emerges when 222 neurodevelopmental trajectories for each of the six cortical layers in 37 Brodmann areas or subareas are parsed into optimal *k*-clusters using *k*-means cluster analysis with the correlation distance as the metric. In this section, we will discuss the members of these *k*-clusters in terms of two distinctive types of members: those individual addresses that have a statistically significant magnitude of change as defined by the expected

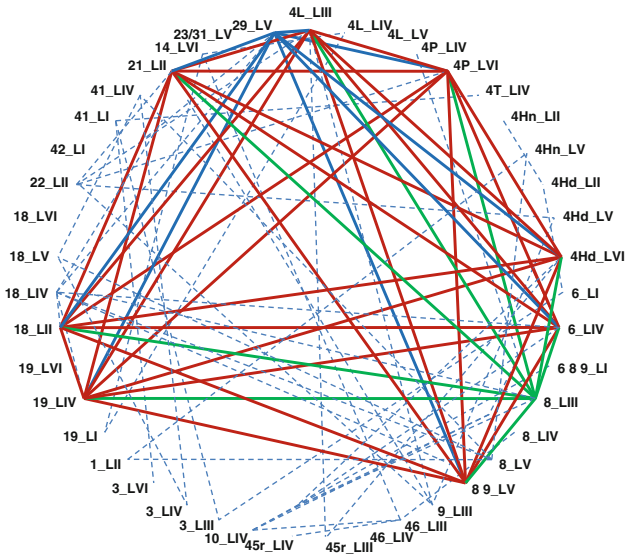

Fig. 7 Relational graph and maximal cliques for K-3 for $D < 0.1$. The 43 addresses in K-3 are listed in clockwise order from BA 4L Layer III at the top to BA 29 LV. The order is the one used by Conel. *Solid red lines* indicate relationships common to both of the two maximal cliques in the K-3 core. *Solid blue lines* show the relational links for BA 29 Layer V, which is the unique address in one of the two maximal cliques. *Solid green lines* show the relational links for BA 8 Layer III, the unique address for the second of the two maximal cliques. Including common and unique nodes, the two maximal cliques have size nine. *Dashed blue lines* indicate the remaining correlation distances with $D < 0.1$. Abbreviations: P = paracentral lobule, T = trunk, Hn = hand

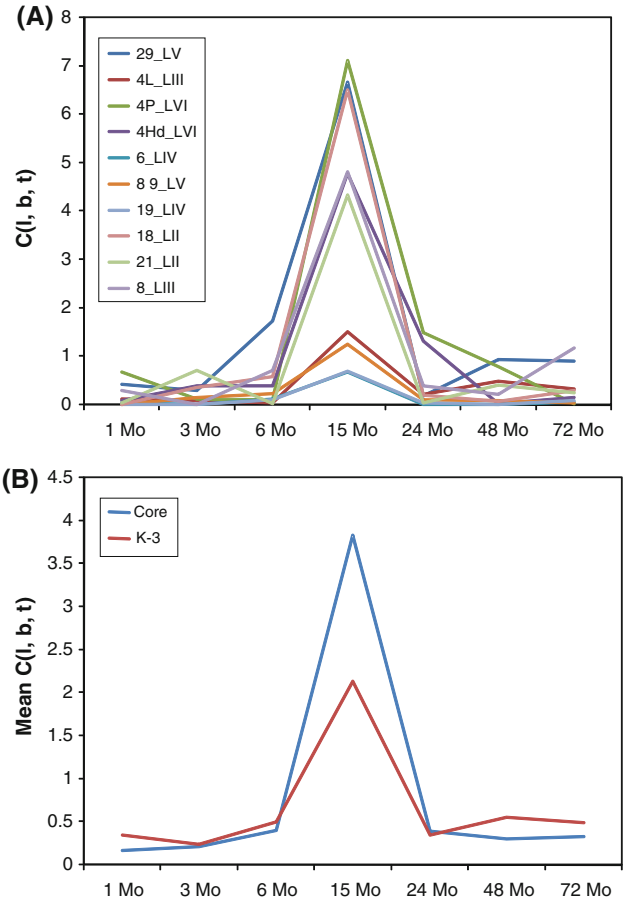

Fig. 8 $C(l, b, t)$ values for K-3 and the K-3 core. **a** $C(l, b, t)$ by change interval for the ten change vector trajectories of the core addresses in K-3. BA 29 LV and BA 8 LIII are the unique nodes in Fig. 7. The eight common addresses in the core are listed between them on the right. The correlated maximum $C(l, b, t)$ values at 15 months occur at multiple scales. **b** Mean $C(l, b, t)$ for the core addresses compared to the mean $C(l, b, t)$ values for the entire k-cluster by change interval

Chi-square distribution of change steps from random mixtures (i.e., $C(l, b, t) > 3.9$), and those addresses whose developmental trajectories define them as part of a totally connected, maximal clique in a given k-cluster (Table 3). As noted at Table 2, maximal clique membership and large magnitude change steps are significantly correlated.

Previous neuroinformatic analysis of Conel's data (Shankle et al. 1998, 2002) employed the statistical methodology known as correspondence analysis across all six types of data reported in Conel: layer width and neuron density (also employed in our present work) as well as somal height and width, large fiber density resulting from Cajal staining and myelinated fiber density resulting from Weigert staining (Shankle et al. 1998). Their method is scale-free and shows a regular developmental pattern from birth to 72 months, with 99% confidence intervals for each cortical area in neocortex overlapping almost completely (Shankle et al. 1998). By contrast to Shankle et al., the $C(l, b, t)$ transformed measurement in our change vector method is normalized across cortical areas and layers and between ages, but is not scale-free.

The evidence for synchronized change in the Conel data comes from three arguments. First, the relative magnitude of the radial spikes in Fig. 4 is not likely an artifact of randomly distributed neuron populations. As described in "Methods", we tested the contrary by making 1,000 random draws from the unit interval for 222 surrogate addresses and eight surrogate observation ages, used Eqs. 1–9 to construct seven k-clusters, and measured the relative size of the spike for each k-cluster to the average change step magnitude for that k-cluster. Comparing the Conel result to the empirical cdf from this process, we estimate the probability of an artifact is rejected with $P \approx 0.001$. Second, we expect a Chi-squared distribution with one degree of freedom to emerge from Eqs. 1 and 3 based on the reasoning in "Methods". This contrasts with Conel's data in Fig. 2, where the distribution mean for $C(l, b, t)$ across all ages is 0.6028 rather than 1 expected from the Chi-square distribution, and the KS test for goodness-of-fit to the Chi-square is rejected with $P = 0.0112$. Finally, The KS test was performed against the null

Table 3 Summary of *k*-cluster cores

Cluster	Maximum clique size	Number	Overlap	Partial overlap	Non-overlap	Maximum $C(l, b, t)$ in change interval
1	4	1	6 LVI 45 LIV 22 LI 24 LIII	–	–	72 Mo
2	6	2	46 LV 45r LV 40 LIII 37 LI 42 LIII	–	41 LIII 10 LIII	1 Mo
3	9	2	4L LIII ***4P LVI**** ***4Hd LVI**** 6 LIV 8 9 LV 19 LIV ***18 LII**** ***21 LII****	–	***29 LV**** ***8 LIII****	15 Mo
4	4	1	7 LIII 40 LIV 22 LIV 21 LVI	–	–	48 Mo
5	4	3	***29 LVI (gp 1/2/3)****	17 LIV (gp 1/3) ***17 LI (gp 1/3)**** 45r LVI (gp 2/3)	37 LII (gp 1) 14 LIII (gp 2) 7 LII (gp 2)	6 Mo
6	4	2	–	–	44 LV (gp 1) 45 LVI (gp 1) **42 LVI (gp 1)*** 13 LI (gp 1) 4P LI (gp 2) 41 LV (gp 2) 38 LVI (gp 2) **14 LI (gp 2)***	24 Mo
7	6	2	6 LIII 6 LV 39 LIV **38 LI*** 13 LIV	–	44 LII 39 LVI	3 Mo

Addresses in bold and marked by an asterisk indicate $C(l, b, t) > 3.9$ ($P < 0.05$, Chi-square test). For K-5, there are three maximal cliques of size four, each partially intersecting the others. The three components are grouped as "gp 1" to "gp 3." K-6 has two maximal cliques of size four that do not intersect, grouped as "gp 1" and "gp 2."

L leg

hypothesis that the normalized neuron population $C(l, b, t)$ is drawn from the same distribution as the previous $C(l, b, t-1)$ at each address. Occurrences of $C(l, b, t)$ that negate this null hypothesis are the statistically significant change step magnitudes that co-occur within the same change step. That is, the null hypothesis is negated by statistically significant synchronized changes to relative neuron population for successive groups of addresses during development. While neuron counts alone are silent as to a potential mechanism, these synchronized changes visible in Fig. 4 at specific addresses that are significantly correlated with *k*-cluster cores ($r = 0.8192$, $P = 0.0242$, two-tailed *t*-test)

imply a clock-like process that produces the synchronization.

The observed synchrony in Fig. 4 is not between selected areas and age, nor selected layer and age, but rather between specific addresses and age. Thus, only BA 6 has four addresses that appear in the maximal clique catalog at Table 3, distributed across three *k*-clusters. Only BA 17 and BA 29 have four addresses, likewise distributed across three *k*-clusters, in Table 2 where large magnitude change steps and maximal clique membership are cross walked. Thus, in addition to area-to-area adjustments known to be significant in postnatal development (Verney et al. 2000), the data also indicate the continued importance of the layer-dominated mammalian prenatal pattern (Butler and Hodos 2005; Noden 1991; Takahashi et al. 1999, etc.), revealing a highly conserved evolutionary pattern (Finlay et al. 2001).

BA 6 is supplementary motor cortex, BA 17 is primary visual cortex (Gazzaniga et al. 2002), and BA 29 (granular retrosplenial cortex) may be involved with the integration of egocentric inputs from the parietal lobe and allocentric representations from the hippocampus and medial temporal lobe (Burgess 2008). This suggests a potential functional role for maximal cliques and the set of unusually large change step addresses that we will take up next.

As noted with Fig. 1, the largest absolute change in raw neuron populations in Conel's data is the drop of 95.9 neurons per sample column that takes place during the change step from 3 to 6 months. The largest relative drop across the cortex (24.55% per sample column) takes place during the next change step from 6 to 15 months. After normalization, the largest values for $C(l, b, t)$ likewise occur during these change steps, as revealed in Table 2. K-3, the largest *k*-cluster with the largest maximal cliques has its maximal changes during the 6–15 months change step. Taking neuron cell death as symptomatic of assimilation and commitment (Stiles 2008), these changes should be consistent with corresponding sensitive periods (e.g., Marcotte and Morere 1990; Ross and Bever 2004; DiCristo et al. 2007).

In humans, these sensitive periods would reasonably be correlated with Piaget's (1952) sensorimotor stage, which extends from birth to 2 years, particularly since this is the Piaget stage that is least subject to environmental factors such as family income or education (Renner et al. 1976). In this context, the change step for 6 months is not surprising. Its three maximal cliques all involve BA29 LVI which has the largest magnitude for $C(l, b, t)$ of any address at any change step. Two of the three maximal cliques contain primary vision address BA17 LI, which also has a large magnitude change value, as well as BA17 LIV. BA17 LIII, associated with color vision processing (Gazzaniga et al. 2002) has statistically significant $C(l, b, t)$ magnitudes in this change step as well as the prior change step at 3 months, where it is a member of the *k*-cluster. According to Piaget (1952), vision is not especially important during the reflex stage immediately after birth, but infants begin to "really look" at things after 1 month, and actively track objects by 2 months. These remaining associations to 6 months remain consistent with continued adaptation and assimilation as called for in Piaget (1952).

This sensorimotor theme continues into the 15 months change step, where the maximal cliques include addresses from primary motor cortex (4L LIII, 4P LVI, 4Hd LVI; Gazzaniga et al. 2002), supplementary motor cortex (BA6 LIV), secondary vision (BA19 LIV and BA18 LII), and the area associated with the frontal eye fields (BA8 LIII; Berman et al. 1999). Retrosplenial cortex also appears in this set (BA29 LV). Primary audition (BA41 LI; Gazzaniga et al. 2002) appears among the large magnitude $C(l, b, t)$ set as well. Six of the ten maximal clique members also have large magnitude change steps.

Mandler (1999) contends that such pre-linguistic primitive steps, particularly kinetic "image-schemas" provide a sufficient conceptual basis on which to build language proper, including such abstract notions as agents, patients, permanent objects, and causation. Tracing backwards from childhood and adult imaging studies to identify key cortical areas for language functions, the *k*-cluster evidence from Conel indicates that these foundations are sometimes laid extremely early during development. Broca's area (BA 44 and 45), associated with language (Broca 1861), appears in three cores with peak $C(l, b, t)$ ranging from 3 months (K-7), very early in language acquisition (Ellison and Semrud-Clikeman 2007), to 24 (K-6) and 72 months (K-1), when children can speak increasingly sophisticated sentences (Tomasello 2003). The earliest of these cores associates BA 44 LII with BA 6 LIII and LV, BA 13 LIV, BA 39 LIV and LVI (area angularis) and BA 38 LI (area temporopolaris). These additional parietal and temporal association areas also show significant activations in fMRI during verb generation tasks (Le Bihan et al. 1993; Cao et al. 1999). BA 39 is associated with Broca's area in word-picture matching among children from 5 to 18 years old (Schmithorst et al. 2007), and semantic processing (Binder et al. 1996). Moreover, BA 39 and superior frontal gyrus, from which the BA 6 samples were drawn in Conel's subjects, form part of a complementary network to the human mirror system, which focuses on the "end" or goal of an action, while the human mirror system appears to focus on the "how" of an action (Hesse et al. 2009). In K-7, BA 44 LII is one of the two non-overlapping addresses, and BA 39 LVI is the other. BA 44 is a recipient of mirror neuron projections (Cadoret et al. 2005). The portion of BA 6 that would have been part of the "classical" human mirror system (Hesse et al. 2009) is von

Economo's area FBop, which was not included in Conel's data. In all of these cases, the timing of the maximum change for the change vectors in K-7 is the 3 months change interval. This is well before most overt manifestations of language or mirror functions, and in agreement with Mandler (1999).

In the remaining cores associated with Broca's area, at 24 months BA 44 LV and BA 45 LVI co-occur with secondary auditory cortex (BA 42, Gazzaniga et al. 2002) and BA 13 (area postcentralis insulae). Direct electrostimulation connects Broca's area with BA 42 (Matsumoto et al. 2004), as does Bayesian analysis of BOLD signals from fMRI for speaker and sentence distinction tasks (Patel et al. 2006). Broca's area and BA 13 are associated in the retention phase of a delayed match-to-sample working memory task (Habeck et al. 2005). Similarly, at 72 months, BA 45 LIV is associated with Wernicke's area (BA 22 LI; Wernicke 1874), supplementary motor (BA 6 LVI, Gazzaniga et al. 2002) and anterior cingulate cortex (BA 24). Broca's area and supplementary motor areas are associated in functional magnetic resonance imaging (fMRI) for noun generation (Cuneod et al. 1995; McArthy et al. 1993), and orthogonal lexical retrieval (Blacker et al. 2006). BA 6 and anterior cingulate cortex are associated for the stimulus and retention phases of delayed match-to-sample working memory (Habeck et al. 2005). BA 22 is also involved in the retention phase (Habeck et al. 2005; Woodward et al. 2006). Broca's and Wernicke's area are both involved in word-picture matching in children between 5 and 18 years old (Schmithorst et al. 2007). Broca's area is associated with supplementary motor and anterior cingulate cortex in morphological tasks related to irregular verbs as well (Sahin et al. 2006). In direct electrostimulation of the cortex in epileptic patients, Broca's and Wernicke's areas demonstrate bidirectional connectivity (Matsumoto et al. 2004).

All of these cited studies associate additional areas outside the *k*-cluster cores, and none has the resolution of an individual cortical address. However, these functional circuits in adult and older juvenile subjects do correspond to the present correlated changes in Conel's neuron population data. We suggest that these patterns in human postnatal neocortical development reflect conserved mechanisms for synchronized functional change steps in postnatal mammalian brain development that are later manifested in behavior.

Keeping in mind our cautionary tale from the Data Supplement that points out the small sample sizes in Conel's work despite the detail he reported at each age, we suggest that similar results can be obtained from animal models. For example, paternally expressed gene 3 (Peg3) mutant mice have a range of deficits, including olfactory function. Inactivation of this gene reduces the incidence of caspase 3 positive cells at 4–6 days postpartum, indicating a reduction in neuron apoptosis. Affected areas in these mice include the bed nucleus of the stria terminalis, nucleus accumbens, caudate putamen, medial pre-optic area, arcuate nucleus, medial amygdala, anterior cortical and posteriodorsal amygdaloid nuclei (Broad et al. 2009). We hypothesize that at least some of these areas would constitute a maximal clique in mice between P4 and P6 if the analogous murine values for $C(l, b, t)$ were calculated from birth to an observation age greater than P6. The associated deficits would emerge later as the mice develop.

Acknowledgments We wish to thank R. S. Shankle for helpful comments and complete access to the CYBERCHILD data base.

References

Abercrombie M (1946) Estimation of nuclear population from microtome sections. Anat Rec 94:239–247

Azevedo FAC, Carvalho LRB, Grinberg LT, Farfel JM, Ferretti REL, Renata EP, Leite REP, Filho WJ, Lent R, Herculano-Houzel S (2009) Equal numbers of neuronal and nonneuronal cells make the human brain an isometrically scaled-up primate brain. J Comp Neurol 513:532–541

Bar I, Goffinet AM (2000) Evolution of cortical lamination: the reelin/Dab1 pathway. In: Bock GR, Cardew G (eds) Evolutionary developmental biology of the cerebral cortex, Novartis Foundation Symposium 228. Wiley, Chichester, pp 114–125

Berman RA, Colby CL, Genovese CR, Voyvodic JT, Luna B, Thulborn KR, Sweeney JA (1999) Cortical networks subserving pursuit and saccadic eye movements in humans: an FMRI study. Hum Brain Mapp 8:209–225

Binder JR, Frost JA, Hammeke TA, Rao SM, Cox RW (1996) Function of the left planum temporale in auditory and linguistic processing. Brain 119:1239–1247

Blacker D, Byrnes ML, Mastaglia FL, Thickbroom GW (2006) Differential activation of frontal lobe areas by lexical and semantic language tasks: a functional magnetic resonance imaging study. J Clin Neurosci 13:91–95

Broad KD, Curley JP, Keverne EB (2009) Increased apoptosis during neonatal brain development underlies the adult behavioral deficits seen in mice lacking a functional paternally expressed gene 3 (Peg3). Dev Neurobiol 69:314–325

Broca P (1861) Sur le principe des localizations cérébrale. Bulletin de la Société d'Anthropologie 2:190–204

Burgess N (2008) Spatial cognition and the brain. Ann N Y Acad Sci 1124:77–97

Butler AB, Hodos W (2005) Comparative vertebrate neuroanatomy: evolution and adaptation, 2nd edn. Wiley, Hoboken

Cadoret G, Mackey S, Petrides M (2005) Orofacial somatomotor responses in the macaque monkey homologue of Broca's area. Nature 435:1235–1238

Cao Y, Vikingstad E, George K, Johnson A, Welch K (1999) Cortical language activation in stroke patients recovering from aphasia with functional MRI. Stroke 30:2331–2340

Conel JL (1939–1967) The postnatal development of the human cerebral cortex, vol 1–8. Harvard University Press, Cambridge

Cuneod C, Bookheimer S, Hertz-Pannier L, Zeffiro T, Theodore W, Le Bihan D (1995) Functional MRI during word generation using conventional equipment: a potential tool for language localization in the clinical environment. Neurology 45:1821–1827

DiCristo G, Chattopadhyaya B, Kuhlman SJ, Fu Y, Bélanger MC, Wu CZ, Rutishauser U, Maffei L, Huang ZJ (2007) Activity-dependent PSA expression regulates inhibitory maturation and onset of critical period plasticity. Nat Neurosci 10:1569–1577

Ellison PAT, Semrud-Clikeman M (2007) Child neuropsychology: assessment and interventions for neurodevelopmental disorders. Springer, New York

Ewens WJ, Grant GR (2001) Statistical methods in bioinformatics: an introduction. Springer, New York

Finlay BL, Darlington RB, Nicastro N (2001) Developmental structure in brain evolution. Behav Brain Sci 24:263–308

Gallego-Diaz V, Schoenwolf GC, Alvarez IS (2002) The effects of BMPs on early chick embryos suggest a conserved signaling mechanism for epithelial and neural induction among vertebrates. Brain Res Bull 57:289–291

Gazzaniga MS, Ivry R, Mangun GR (2002) Cognitive neuroscience: the biology of the mind, 2nd edn. WW Norton, New York

Gentle JE (2002) Elements of computational statistics. Springer, New York

Godsil C, Royle G (2004) Algebraic graph theory. Springer, New York

Gohlke JM, Griffith WC, Faustman EM (2007) Computational models of neocortical neuronogenesis and programmed cell death in the developing mouse, monkey, and human. Cereb Cortex 17:2433–2442

Habeck C, Rakitin BC, Moeller J, Scarmeas N, Zarahn E, Brown T, Stern Y (2005) An event-related fMRI study of the neural networks underlying the encoding, maintenance, and retrieval phase in a delayed-match-to-sample task. Cogn Brain Res 23: 207–220

Hesse MD, Sparing R, Fink GR (2009) End or means—the "what" and "how" of observed intentional actions. J Cogn Neurosci 21:776–790

Holland PWH, Takahashi T (2005) The evolution of homeobox genes: implications for the study of brain development. Brain Res Bull 66:484–490

Huang EJ, Reichardt LF (2001) Neurotrophins: roles in neuronal development and function. Annu Rev Neurosci 24:677–736

Kolpak A, Zhang J, Bao ZZ (2005) Sonic hedgehog has a dual effect on the growth of retinal ganglion axons depending on its concentration. J Neurosci 25:3432–3441

Le Bihan D, Jezzard P, Turner R, Cuneod C, Zefferio T (1993) Analysis of functional brain MR images with Z maps. J Magn Reson Imaging 3:141

Letinic K, Zoncu R, Rakic P (2002) Origin of GABAergic neurons in the human neocortex. Nature 417:645–649

Mandler JM (1999) Preverbal representation and language. In: Bloom P, Peterson MA, Nadel L, Garrett MF (eds) Language and space. MIT, Cambridge, pp 365–384

Marcotte AC, Morere DA (1990) Speech lateralization in deaf populations: evidence for a developmental critical period. Brain Lang 39:134–152

Matsumoto R, Nair DR, LaPresto E, Najm I, Bingaman W, Shibasaki H, Lueders HO (2004) Functional connectivity in the human language system: a cortico-cortical evoked potential study. Brain 127:2316–2330

McArthy G, Blamire A, Rothman D, Gruetter R, Schulman R (1993) Echoplanar magnetic resonance imaging studies of frontal cortex activation during word generation in humans. Proc Natl Acad Sci USA 90:4592–4596

Michel GF, Tyler AN (2005) Critical period: a history of the transition from questions of when, to what, to how. Dev Psychobiol 46: 156–162

Noden DM (1991) Vertebrate craniofacial development: the relation between ontogenetic process and morphological outcome. Brain Behav Evol 38:192–225

Nomura T, Takahashi M, Hara Y, Osumi N (2008) Patterns of neurogenesis and amplitude of reelin expression are essential for making a mammalian-type cortex. Plos One 1:e1454

Patel RS, Bowman FD, Rilling JK (2006) Determining hierarchical functional networks from auditory stimuli fMRI. Hum Brain Mapp 27:462–470

Piaget J (1952) The origins of intelligence in children. International Universities Press, New York

Pilati N, Barker M, Panteleimonitis S, Donga R, Hamann M (2008) A rapid method combining Golgi and Nissl staining to study neuronal morphology and cytoarchitecture. J Histochem Cytochem 56:539–550

Rakic P (1988) Specification of cerebral cortical areas. Science 241: 170–176

Rakic P (2001) Neurobiology: neurocreationism—making new cortical maps. Science 294:1011–1012

Renner J, Stafford D, Lawson A, McKinnon J, Friot E, Kellogg D (1976) Research, teaching,nd learning with the Piaget model. University Oklahoma Press, Norman

Ross DS, Bever TG (2004) The time course for language acquisition in biologically distinct populations: evidence from deaf individuals. Brain Lang 89:115–121

Sahin NT, Pinker S, Halgren E (2006) Abstract grammatical processing of nouns and verbs in Broca's area: evidence from fMRI. Cortex 42:540–562

Schmithorst VJ, Holland SK, Plante E (2007) Object identification and lexical/semantic access in children: a functional magnetic resonance imaging study of word-picture matching. Hum Brain Mapp 28:1060–1074

Shankle RS, Romney AK, Landing BH, Hara J (1998) Developmental patterns in the cytoarchitecture of the human cerebral cortex from birth to 6 years examined by correspondence analysis. Proc Natl Acad Sci USA 95:4023–4028

Shankle RS, Landing BH, Rafii MS, Hara J, Fallon JH, Romney AK, Boyd JP (2000) CYBERCHILD: a database of the microscopic development of the postnatal human cerebral cortex from birth to 72 months. Neurocomputing 32–33:1109–1114

Shankle RS, Hara J, Fallon JH, Landing BH (2002) How the brain develops and how it functions: application of neuroanatomical data of the developing human cerebral cortex to computational models. In: Ascoli AA (ed) Computational neuroanatomy: principals and methods. Humana, Totowa, pp 402–436

Stiles J (2008) The fundamentals of brain development: integrating nature and nurture. Harvard University Press, Cambridge

Takahashi T, Goto T, Miyame S, Nowakowski RS, Caviness VS Jr (1999) Sequence of neuron origin and neocortical laminar fate: relation to cell cycle of origin in the developing murine cerebral wall. J Neurosci 19:10357–10371

Tomasello M (2003) Constructing a language: a usage-based theory of language acquisition. Harvard University Press, Cambridge

Verney C, Takahashi T, Bhide PG, Nowakowski RS, Caviness VS Jr (2000) Independent controls for neocortical neuron production and histogenetic cell death. Dev Neurosci 22:125–138

von Economo CB, Koskinas GN (1925) The cytoarchitectonics of the adult human cortex. Springer, Vienna

Wernicke K (1874) Der aphasische Symptomencomplex. Eine psychologische Studie auf anatomischer Basis. M. Crohn und Weigert, Breslau

Wilks SS (1962) Mathematical statistics. Wiley, New York

Woodward TS, Cairo TA, Ruff CC, Takane Y, Hunter MA, Ngan ETC (2006) Functional connectivity reveals load dependent neural systems underlying encoding and maintenance in verbal working memory. Neuroscience 139:317–325